

## FORMATION OF PAHS AND CARBONACEOUS SOLIDS IN GAS-PHASE CONDENSATION EXPERIMENTS

C. JÄGER<sup>1</sup>, F. HUISKEN

Max-Planck-Institut für Astronomie, Königstuhl 17, D-69117 Heidelberg and Institut für Festkörperphysik, Helmholtzweg 3, D-07743 Jena, Germany

H. MUTSCHKE, I. LLAMAS JANSA

Astrophysikalisches Institut und Universitäts-Sternwarte (AIU), Schillergässchen 2-3, D-07745 Jena, Germany

TH. HENNING

Max-Planck-Institut für Astronomie, Königstuhl 17, D-69117 Heidelberg, Germany

*accepted for publication in ApJ*

### ABSTRACT

Carbonaceous grains represent a major component of cosmic dust. In order to understand their formation pathways, they have been prepared in the laboratory by gas-phase condensation reactions such as laser pyrolysis and laser ablation. Our studies demonstrate that the temperature in the condensation zone determines the formation pathway of carbonaceous particles. At temperatures lower than 1700 K, the condensation by-products are mainly polycyclic aromatic hydrocarbons (PAHs), that are also the precursors or building blocks for the condensing soot grains. The low-temperature condensates contain PAH mixtures that are mainly composed of volatile 3-5 ring systems. At condensation temperatures higher than 3500 K, fullerene-like carbon grains and fullerene compounds are formed. Fullerene fragments or complete fullerenes equip the nucleating particles. Fullerenes can be identified as soluble components. Consequently, condensation products in cool and hot astrophysical environments such as cool and hot AGB stars or Wolf Rayet stars should be different and should have distinct spectral properties.

*Subject headings:* astrochemistry, dust, carbon soot, molecules, polycyclic aromatic hydrocarbons, laser ablation, infrared extinction, UV/visible extinction

### 1. INTRODUCTION

It is generally assumed that most of the primary cosmic carbonaceous material is formed as nano- and subnanometer-sized particles via gas-phase condensation in envelopes of carbon-rich asymptotic giant branch (AGB) stars (Henning & Salama 1998). The very probable and abundant precursor for this process is acetylene (C<sub>2</sub>H<sub>2</sub>). The presence of a solid nanosized carbonaceous material in addition to molecular polycyclic aromatic hydrocarbons (PAHs), which are considered to be the carriers of the aromatic IR (AIR) bands in different astrophysical environments, is sufficiently proven by the IR excess emission of transiently heated grains (Boulanger et al. 1998; Draine & Li 2001). However, a firm detection of individual band carriers for the AIRs has not been succeeded. The role of fullerenes as possible band carriers remains uncertain. Giant fullerenes were already found in primitive meteorites (Smith & Buseck 1981; Buseck 2002). The detection of fullerenes in astronomical environments is still a matter of debate (Foing & Ehrenfreund 1997; Galazutdinov et al. 2000; Nuccitelli et al. 2006; Sellgren et al. 2007).

Several authors (Frenklach & Feigelson 1989; Cherchneff et al. 1992; Allain et al. 1997) have modeled the formation of PAHs in AGB stars. Whereas these authors determined a narrow temperature range of 900 to 1100 K for the formation of PAHs in circumstellar

environments, Cherchneff & Cau (1999) reconsidered the modeling of the PAH and carbon dust formation in carbon-rich AGB stars. They developed a physico-chemical model, which describes the periodically shocked gas in the circumstellar shells close to the photosphere of the stars. The authors found that benzene (C<sub>6</sub>H<sub>6</sub>) formation begins at 1.4 R<sub>\*</sub> and, at a radius of 1.7 R<sub>\*</sub>, the conversion of single rings to PAHs starts at a temperature of around 1700 K. This temperature is much higher than the temperature window calculated in previous studies.

Temperatures and pressures in circumstellar condensation environments are uncertain since they depend on various model assumptions, for instance, mass loss rates, gas density outflow velocity, and dust formation. Pulsations of the helium burning shells affect the atmospheres and can cause shock fronts, which result in density/pressure fluctuations (Nowotny et al. 2005a). Pressure ranges of 0.03–100 and 1–800 dyn/cm<sup>2</sup> (3×10<sup>-5</sup>–0.1 and 1×10<sup>-3</sup>–0.8 mbar) for AGB stars with an effective temperature of 2500 and 4000 K, respectively, have been calculated (Lederer et al. 2006).

One important way to successfully understand the condensation of dust in astrophysical environments is to calculate the stability limits for condensation of dust species based on chemical models and different chemical and physical parameters. Lodders & Fegley (1999) have modeled the condensation of carbonaceous grains in dust-forming shells of carbon-rich AGB stars using pres-

Electronic address: Cornelia.Jaeger@uni-jena.de

<sup>1</sup> Corresponding author

tures between 10 and  $3 \times 10^3$  dynes/cm<sup>2</sup> (0.01-3 mbar). The authors found that the condensation temperatures generally decrease with decreasing total pressure. However, graphite is an exception since the condensation temperature is not pressure-dependent but sensitive to the C/O ratio in the dust-forming zone. Higher C/O ratios shift the pressure range to higher values.

For hydrogen-poor Wolf Rayet (WR) stars with high effective temperatures between 20,000 and 90,000 K, running through the WC phase, the carbon dust condensation is supposed to start with small carbon chains, that can form monocyclic rings (von Helden et al. 1993). These carbon chains and rings represent the precursors for fullerenes, which finally form the amorphous carbon grains (Cherchneff et al. 2000). In this scenario, the PAHs are ruled out as possible intermediates.

It is imperatively assumed that the formation pathway of carbon condensation determines the resulting structure, chemical composition, and morphology of the condensing grains. Therefore, it is important to know the formation process of cosmic dust grains and possible precursors and/or intermediates such as PAHs, fullerenes, or polyyne carbon chains, in order to understand their spectral properties in different astrophysical environments.

Despite all efforts, the formation process of carbon nanoparticles in astrophysical environments and even in terrestrial carbon condensation processes is not sufficiently understood. Most studies of soot formation pathways have been performed on premixed gas flames or laminar diffusion flames. The formation of PAHs and nanometer-sized carbon grains in fuel-rich hydrocarbon flames has been extensively investigated by Burtscher (1992), Baum et al. (1992), and Weilmünster et al. (1999). The chemical species associated with the early stage of soot growth and soot precursor particles in flames have been studied by Dobbins et al. (1998) and Öktem et al. (2005). Homann (1998) claimed that, by association of two or more large PAHs in form of biaryl or  $\pi$  complexes, a new group of PAHs is formed, which he called aromers. These aromers are supposed to be precursors for fullerenes and soot particles. The disadvantage of studying soot formation in flames is the varying temperature and chemistry in the flames that seems to be associated with changes in the particle formation pathways.

We have employed gas-phase condensation experiments to produce nanometer- and subnanometer-sized carbonaceous particles within two different temperature regimes, a high-temperature (HT) and low-temperature (LT) condensation regime. Both gas-phase condensation techniques come close to the grain formation process suggested to occur in astrophysical environments. The study of the formation pathways has been performed experimentally by analytical characterization of the soot and its by-products, including high-resolution transmission electron microscopy (HRTEM), chromatographic methods, and mass spectroscopy. Finally, the spectral properties of the two different condensates have been measured from the far UV (FUV) to the infrared (IR), in order to compare their spectral characteristics. They are discussed in § 3.2.

The synthesis conditions for all series of gas-phase condensation experiments are presented in Table 1. The first two rows refer to the high-temperature (HT) condensation experiments performed with pulsed lasers characterized by high power densities and, consequently, high temperatures of more than 3500 K in the condensation zone. The last four rows of Table 1 describe the low-temperature (LT) condensation experiments that process at temperatures lower than 1700 K. The last column of the table contains a description of the two types of condensed carbonaceous matter.

For HT condensations, laser ablation of graphite with subsequent condensation of carbonaceous matter in quenching gas atmospheres of He or He/H<sub>2</sub> (3/2 He/H<sub>2</sub> standard volume flow) mixtures at pressures between 3.3 and 26.7 mbar has been applied. The second harmonic of a pulsed Nd:YAG laser was used to evaporate carbon from a graphite target. The pressure was kept as low as possible to come close to the conditions in astrophysical condensation zones. However, at a pressure lower than 3.3 mbar, the condensation rate became too slow to be manageable for the condensation of grains. In order to study the influence of the pressure on the composition and final structure of the condensate, we have increased the pressure up to 26.7 mbar. In addition, laser-induced pyrolysis (LIP) of gas-phase hydrocarbon precursors (ethylene, acetylene, and benzene) at pressures around 335 mbar using a pulsed CO<sub>2</sub> laser have been carried out. In such a condensation experiment, the pressure has to be higher in order to obtain a stable flame and constant condensation conditions. In the table, the terms LA (laser ablation) and LPPL (laser pyrolysis, pulsed laser) refer to a number of different experiments with varying laser power densities, quenching gas mixtures, pressures, and precursors. The condensing particles were extracted from the condensation zone by using a molecular beam technique and deposited on KBr and CaF<sub>2</sub> substrates for IR and UV/visible spectroscopy, respectively. A more detailed description of both methods can be found in Llamas-Jansa et al. (2007) and Jäger et al. (2008b). For all the HT experiments, the laser power densities were varied between  $1 \times 10^7$  and  $9 \times 10^9$  W cm<sup>-2</sup>, which is a measure that correlates with the temperature in the condensation zone. For HT gas-phase condensation processes of nanoparticles, we can provide lower limits of the temperature in the condensation zone. The vibrational temperature of the laser-induced plasma generated by laser evaporation of a graphite target in a 10 mbar He atmosphere was found to range between 4000 and 6000 K for power densities between  $5 \times 10^8$ – $2 \times 10^9$  W cm<sup>-2</sup> (Iida & Yeung 1994). In the LIP of hydrocarbons, the employed power densities are only slightly lower compared to the ablation experiments and, therefore, the condensation temperatures are well comparable, which is confirmed by other authors (Kojima & Naito 1981; Doubenskaia et al. 2006).

LT condensation studies have been performed by laser-induced pyrolysis (LIP) of gas-phase hydrocarbon precursors, such as ethylene, acetylene, and benzene, at pressures around 750 mbar, applying a continuous-wave (cw) CO<sub>2</sub> laser. The detailed experimental setup is described elsewhere (Jäger et al. 2006, 2007). The condensed nanoparticles have been collected in a filter. The

terms LPcw2–LPcw5 refer to individual condensation experiments performed by application of laser pyrolysis with a cw CO<sub>2</sub> laser. For the LT condensation experiments, the laser power densities varied between 850 and 6400 W cm<sup>-2</sup>. The power densities are orders of magnitude lower compared to the HT condensations and, therefore, the corresponding temperatures in the condensation zone are much lower and were found to be in the range between 1000 and 1700 K. In these experiments, the temperatures have been determined with a pyrometer.

For both, HT and LT condensations, the pressures considerably exceeded the pressure ranges supposed to be valid in the condensation zone of AGB stars. In laboratory experiments it is necessary to scale up the pressure since the free path lengths of atoms and clusters would be too long for the laboratory setup at pressures lower than 1 mbar. Therefore, in order to simulate the condensation of particles, we have to scale up the applied pressure ranges in the condensation apparatus at least by 1-2 orders of magnitude. However, we would like to point out that the total pressures provided in Table 1 do not represent the partial pressures of the condensing species since we additionally use a quenching gas such as helium or hydrogen. The real partial pressure of the condensing carbon species cannot be measured. Therefore, an exact determination of the ratio between the partial and the equivalent pressure of the gaseous carbon species, which is related to the supersaturation factor (see § 3), during the condensation process is very difficult.

The internal structures of the condensed carbon particles and the formation of possible intermediates and by-products were investigated with high-resolution transmission electron microscopy (HRTEM) (JEOL JEM 3010 microscope) operating at an acceleration voltage of 300 kV. The soluble components of the condensates were removed by soxhlet extraction in toluene. The composition of the extracts and condensates was characterized by using gas chromatographic/mass spectrometric (GC/MS) analyses, high-performance liquid chromatography (HPLC) combined with a UV/visible diode array detector, and matrix-assisted laser desorption/ionization in combination with time-of-flight mass spectrometry (MALDI-TOF). Technical details of the analytical and spectral analyses are provided in previous papers (Jäger et al. 2006, 2008b).

### 3. RESULTS AND DISCUSSIONS

#### 3.1. Soot Formation at Different Temperatures

HRTEM images of the carbonaceous matter produced in a HT gas-phase condensation process are shown in Figure 1. A much more detailed chemical and structural description of the HT condensates can be found in Llamas-Jansa et al. (2007) and Jäger et al. (2008b). The HRTEM micrographs reveal that, in addition to individual fullerenes, which are marked by arrows in Figure 1a, very small fullerene-like particles are produced. These particles are composed of small, strongly bent graphene layers with varying lengths and distances between these layers. The level of disorder depends on the employed condensation conditions. Soot condensates containing low amounts of hydrogen show more ordered and frequently closed fullerene cages (Figure 1c) whereas grains with higher hydrogen contents are less ordered and do

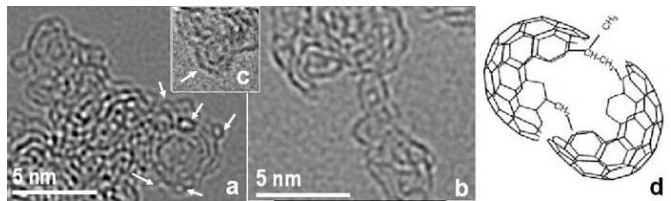


FIG. 1.— HRTEM images of fullerene-like nanoparticles generated in a HT condensation process (samples from series LA). In image (a), fullerene and elongated fullerene molecules are marked by arrows. Image (b) and (c) present a typical fullerene cage fragment and a buckyion with two interleaved fullerene cages (size 1.7 nm, also marked by an arrow), respectively. Model (d) illustrates the likely link between fullerene fragments in the soot grains.

not show completely closed cages. In these grains, the cage fragments stick together by van der Waals forces or are linked by aliphatic  $-\text{CH}_x$  groups (see sketch d in Figure 1).

Both methods of HT condensation (laser ablation and laser pyrolysis) work at different pressures. However, the increase of the pressure in the condensation zone by two orders of magnitude does not result in a change of the structure of the condensate.

The small size of the grains points to a strong supersaturation of the carbon vapor in the condensation zone resulting in a high number of nucleation seeds. This is based on the assumption that, generally, homogeneous nucleation needs a high supersaturation of the vapor phase (Granquist & Buhrman 1976; Heidenreich et al. 2003). The relation between the size of the critical grains  $r^*$  and the Gibbs free energy is defined by the equation  $r^* = -2\gamma/\Delta G_v$ , where  $\gamma$  stands for the surface energy of the condensed species (Cao 2004). The Gibbs free energy  $\Delta G_v$  is again proportional to the temperature  $T$  and the supersaturation  $S$  via the relation  $\Delta G_v = \frac{-kT}{\Omega} \ln(1 + S)$  where  $k$  is the Boltzmann constant and  $\Omega$  is the atomic volume. Therefore, in order to reduce the critical size of stable nuclei in the condensation zone, which is a requirement for the production of small grains, one needs to increase the Gibbs free energy  $\Delta G_v$  of nucleation per unit volume. TEM micrographs of the HT samples partly show the appearance of larger particles up to 10 nm, which were formed by coagulation of the original, very small fullerene-like carbon grains. Under these condensation conditions (high supersaturation and temperature), it is supposed that the further particle growth is exclusively due to coagulation.

The generation of fullerenes and fragments of them in the condensation process could be verified by using electron microscopy. The presence of symmetric and elongated fullerene molecules with different numbers of carbon atoms is clearly visible in the HRTEM micrographs. The symmetric fullerenes range from 0.5 up to 1.03 nm corresponding to fullerenes from C<sub>36</sub> up to C<sub>130</sub> (Goel et al. 2004). A soot formation process via polyene chains, fullerenes and fullerene snatches, respectively, was already proposed by Kroto & McKay (1988). MALDI-TOF studies of the HT condensate have shown that no PAHs are formed as intermediates.

The critical point in the creation of bent graphene layers or disturbed fullerene-like structures is the formation of cage fragments or molecules from the chains. Quantum chemical molecular dynamics simulations have demonstrated that high carbon densities are essential for

TABLE 1

EXPERIMENTAL CONDITIONS COMPRISING THE HT AND LT GAS-PHASE CONDENSATION EXPERIMENTS. THE TERMS LA AND LPPL DENOTE A SERIES OF EXPERIMENTS PERFORMED AT HIGH TEMPERATURES, BUT WITH VARYING CONDITIONS. THE TERMS LPCWI DESCRIBE INDIVIDUAL LT CONDENSATION EXPERIMENTS. A MORE DETAILED DESCRIPTION OF THESE EXPERIMENTS CAN BE FOUND ELSEWHERE (LLAMAS-JANSA ET AL. 2007; JÄGER ET AL. 2008B).

| Experiment | Precursor   | Buffer gas        | Laser  | Laser power density ( $\text{W cm}^{-2}$ ) | Temperature (K) | Condensate                         |
|------------|---|-------------------|--------|--|-----------------|------------------------------------|
| LA         | Graphite  | He/H <sub>2</sub> | pulsed | $2 \times 10^8 - 9 \times 10^9$            | $\geq 4000$     | fullerene-like soot and fullerenes |
| LPPL       | C <sub>2</sub> H <sub>4</sub> , C <sub>2</sub> H <sub>2</sub> , C <sub>6</sub> H <sub>6</sub> | He/Ar             | pulsed | $1 \times 10^7 - 1 \times 10^9$            | $\geq 3500$     | fullerene-like soot and fullerenes |
| LPcw2      | C <sub>2</sub> H <sub>4</sub> , C <sub>2</sub> H <sub>2</sub>                                 | Ar                | cw     | 5200                                       |                 | soot and 14 wt% PAHs               |
| LPcw3      | C <sub>2</sub> H <sub>4</sub> , C <sub>6</sub> H <sub>6</sub>                                 | Ar                | cw     | 5200                                       | $\sim 1500$     | soot and 33 wt% PAHs               |
| LPcw4      | C <sub>2</sub> H <sub>4</sub> , C <sub>6</sub> H <sub>6</sub>                                 | Ar                | cw     | 6400                                       | $\sim 1700$     | soot and 17 wt% PAHs               |
| LPcw5      | C <sub>2</sub> H <sub>4</sub>   | Ar                | cw     | 850  | $\sim 1000$     | 100 wt% PAHs                       |

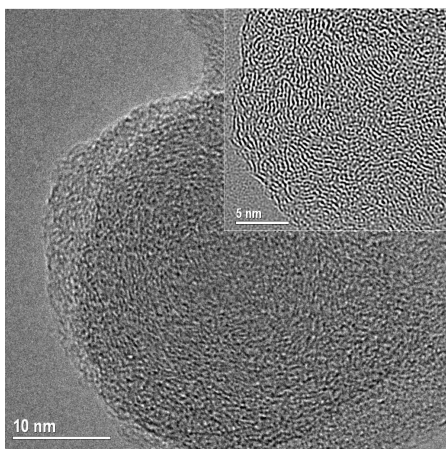


FIG. 2.— HRTEM image of a typical large carbon nanoparticle produced in a LT process (LPcw2-4). The inset displays a section of a particle showing the arrangement and mean sizes of the graphene layers.

such processes, which can be found for example in carbon arc or laser ablation processes (Zheng et al. 2005). These authors found that the C<sub>2</sub> molecules quickly combine to long and branched carbon chains and macromolecules for temperatures above 2000 K, which form small cyclic structures with long carbon chains attached (nucleation). The second step is a further ring condensation growth for example between two linear chains attached to a nucleus. Consequently, fullerene fragments of bowl shape with side chains are formed in this step (Irle et al. 2003). Furthermore, coalescence reactions of small fullerenes (Yeretzian et al. 1993) can result in the formation of larger and elongated fullerene cages, which have also been observed by HRTEM.

In contrast, the condensed grains in LT processes are much larger and show more ordered and well developed planar graphene layers inside the particles (see Figure 2). Additionally, mixtures of PAHs were formed as by-products. These soluble components were extracted from the soot, and the constituents of the extract were identified by chromatographic methods. A mixture of around 70 different PAHs, partly hydrogenated at the edges, could be identified using GC/MS and HPLC. PAHs with 3-5 ring systems are by far the most abundant components. PAHs with masses up to 3000 Da were also detected by application of MALDI-TOF mass spec-

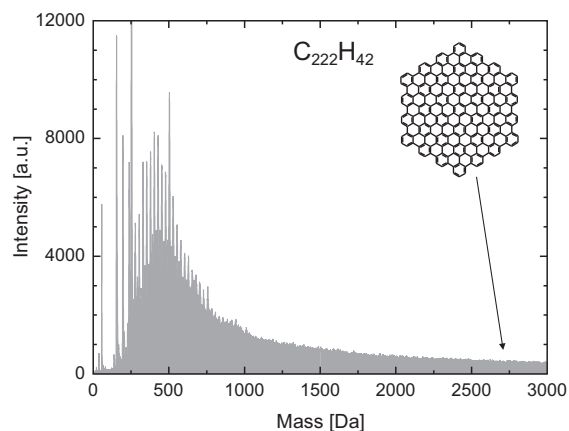


FIG. 3.— MALDI TOF spectrum of the LT soot sample LPcw3 showing that PAHs with masses up to 3000 Da are observed. The individual peaks show abundant PAHs of lower masses. To exemplify a PAH molecule with comparable mass, a symmetric molecule comprising 91 condensed rings and having a diameter of about 3 nm is presented.

troscopy (see Figure 3), but only in very small amounts. The large size and high internal order of the condensed soot grains points to a low supersaturation of the carbon vapor and the formation of a smaller number of stable nuclei compared to the HT condensation process. In the LT condensation, the further particle growth is dominated by condensation of intermediates on the surface of the seeds, which means that PAHs continuously accumulate on the surface of the grains. Since larger PAHs have a lower volatility compared to the smaller ones, a preferred accumulation of large molecules during the surface growth process can be observed. The accumulation of the large molecules on the surfaces of the seeds can be confirmed by a detailed analysis of the HRTEM micrographs revealing a mean length of the graphene sheets inside the particles of around 1.8 nm corresponding to PAHs with masses of around 1000 Da. However, the longest graphene layers that could be determined in the micrographs of the soot particles had extensions of about 3 nm, which corresponds to the highest-mass PAHs detected with MALDI-TOF measurements.

### 3.2. Spectroscopic Properties of the LT and HT Condensates

The spectral properties of the HT and LT condensates in the UV/visible range differ considerably. Although the HT soot grains consist of about 50%  $sp^2$  hybridized carbon atoms, the UV spectra do not show distinct UV absorption bands (see Figure 4). However, a deconvolution of the UV/visible absorption profile by employing four Gaussians reveals weak and broad bands due to  $(\pi-\pi^*)$  transitions between  $4.45$  and  $3.84\mu\text{m}^{-1}$  depending on the hydrogen content. The width of the  $(\pi-\pi^*)$  main band and the appearance of a plasmon band around  $2.5\mu\text{m}^{-1}$  ( $400\text{nm}$ ) accounts for a certain disorder in the carbon structures due to a broad distribution of curvatures and lengths of graphene layers in the small fullerene-like carbon grains (Jäger et al. 2008b,c). A very weak band around  $5.2\mu\text{m}^{-1}$  ( $190\text{nm}$ ) can be attributed to the absorption of  $-\text{C}=\text{O}$  groups.

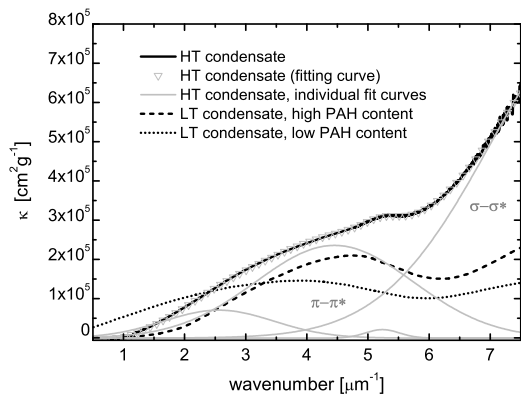


FIG. 4.— UV/visible spectra of selected LT and HT condensate samples. The HT soot sample (black curve) has been produced in 6.0 mbar He/H<sub>2</sub> atmosphere by laser ablation ( $H/C=0.52$ ). The solid gray curves represent 4 individual Gaussian profiles fitting as a sum the absorption profile. The dashed and dotted black curves show the UV/visible spectra of two LT condensates containing a high and low amount of the soluble organic component, respectively (see text).

In contrast to the HT grains, the soot grains in the LT condensate have much higher content of  $sp^2$  hybridized carbon atoms which was found to range between 80 and 92% (Jäger et al. 2008a). The UV spectra of LT condensates with very similar grain structure and composition (soot and PAH mixtures) produced by propane combustion (Schnaiter et al. 2006; Llamas Jansa et al. 2008) are shown in Figure 4. The condensates do show distinct UV absorption bands caused by  $(\pi-\pi^*)$  transitions ranging between  $3.6$  and  $4.9\mu\text{m}^{-1}$  ( $204$  and  $256\text{nm}$ ). The exact position of this band depends on the internal structure of the soot grains and the content and composition of the soluble PAH component, which also contributes to the spectrum. The spectrum with the band position at  $3.6\mu\text{m}^{-1}$  belongs to a condensate consisting of more than 90% soot. Here the band position is dominated by the soot fraction and shows a strongly enhanced absorption in the visible range. The second LT spectrum is typical for a composite consisting of a high amount of PAHs (around 50%) and a smaller fraction of soot grains. The sizes and the internal structure of the grains are strongly comparable in both condensates. Therefore, the differ-

ence in the positions of the  $(\pi-\pi^*)$  transitions is caused by the varying PAH content.

Spectral observations of carbon-rich late-type stars in the UV range, the places where grain condensation is expected, are limited since such stars are too cool to be observable in this range. Post AGB stars and planetary nebulae are brighter in the UV, but due to the strong rise of temperature, the originally produced dust has already been processed (Kwok et al. 1999).

The UV spectrum recorded for the active mass-losing and dust-producing post AGB star HD 44179, recently presented by Vijn et al. (2005), shows a very broad hump with a maximum near  $200\text{nm}$  ( $5\mu\text{m}^{-1}$ ) which is in width and position similar to the UV spectrum for the LT condensate containing a high amount of PAHs (dashed curve in Figure 4). The effective temperature of the star amounted to  $8000\text{K}$ , but the measured blue luminescence points to the presence of small PAHs. Possibly similar to the measured UV spectrum in HD 44179 is the one in the hydrogen-rich post AGB star HD 89353 (Buss et al. 1989) with an effective temperature of  $7500\text{K}$  (Monier & Parthasarathy 1999). Aromatic IR bands, observable in both objects, suggest the presence of PAHs or aromatic subunits in the carbonaceous dust which probably result from the processing of the original dust that is supposed to start with the end of the AGB phase (Kwok et al. 1999).

In the hydrogen-poor post AGB star HD 213985 (Buss et al. 1989) and in the R Coronae Borealis variable stars (R CrB and V 348 Sgr) (Hecht et al. 1984; Drilling & Schönberner 1989; Drilling et al. 1997), UV band positions at  $230$  ( $4.34\mu\text{m}^{-1}$ ) and  $250\text{nm}$  ( $4.0\mu\text{m}^{-1}$ ) were observed, respectively, that are comparable to UV spectral bands measured for LT condensates but with low PAH content. Indeed, these objects do not show aromatic IR bands.

The IR spectral properties of the HT condensates are characterized by strong saturated and aliphatic  $-\text{CH}_x$  absorptions at  $3.4$ ,  $6.8$ , and  $7.25\mu\text{m}$ . This supports the assumption that saturated aliphatic  $-\text{CH}_x$  groups are mainly responsible for the links between the fullerene fragments (compare Figure 1d). No aromatic  $=\text{C}-\text{H}$  stretching vibrational bands at  $3.3\mu\text{m}$  have been observed, but aromatic  $-\text{C}=\text{C}-$  groups can be identified between  $6.2$  and  $6.25\mu\text{m}$ . Additionally, out-of-plane bending vibrations of aromatic  $=\text{C}-\text{H}$  groups are observed between  $11$  and  $14\mu\text{m}$ , since their intensity is higher than the intensity of the stretching bands. A weak feature at  $5.8\mu\text{m}$  can be attributed to a small amount of  $-\text{C}=\text{O}$  groups inside the carbon structure, but also higher fullerenes can show vibrational modes in this range (Mordkovich 2000). Interestingly, signatures for the presence of  $-\text{C}\equiv\text{C}-$  triple bonds can be observed in the in situ IR spectra of the HT condensates at  $3.03$  and  $4.7\mu\text{m}$ , which points to the formation of polyynes as intermediates and supports the idea about the formation of fullerene snatches. A more detailed description of the IR spectral properties of these particles produced in HT condensations can be found in Jäger et al. (2008b).

LT condensates, that represent a mixture of soot and PAHs, show aromatic IR bands (AIBs) as well as aliphatic IR band, with both types being partly superimposed on two broad plateau features around  $8$  and

12  $\mu\text{m}$  (see Figure 5). In the spectra, quite a number of partly small, individual bands can be recognized. However, a firm separation of aliphatic and aromatic IR features in the 6–10  $\mu\text{m}$  range and an attribution of every IR band to a special functional group of specific components in this range is difficult and suffers from the fact that the soluble component of the condensate contains around 70 different aromatic species which can be partly hydrogenated. In addition, the structural variety of the grains and their functional groups becomes manifest in additional IR bands.

The non-treated condensate (see dashed curve) shows aromatic bands at 3.3, 6.27, 6.35, 6.88, 7.22, 7.93, 8.47, 8.65, 9.28, 9.72, 10.50, 11.36, 11.9, 12.05, 12.14, 12.30, 13.27, 13.56, and 14.30  $\mu\text{m}$  as well as aliphatic IR bands at 3.4, 6.75, 6.94, 7.01, and 7.5  $\mu\text{m}$ . The bands beyond 6.7  $\mu\text{m}$  mainly arise from  $-\text{C}-\text{C}-$  stretching and  $\text{C}-\text{H}$  deformation bands. In this spectral range a firm assignment of an IR band to a specific functional group is very difficult even for carbonaceous grains without adsorbed PAHs which may contain a lot of different functional groups with single and double bonds integrated in varying chemical environments leading to a distribution of vibrational bands in this spectral range. IR bands at wavelengths larger than 11  $\mu\text{m}$  can be assigned to aromatic  $=\text{C}-\text{H}$  out-of-plane bending vibrations. In particular, the bands at 13.27, 13.56, and 14.3  $\mu\text{m}$  are caused by 4-5 adjacent H atoms bound to the aromatic ring and argue for smaller PAHs, PAHs with outer rings containing 4 hydrogen, or for special PAHs containing phenyl rings bound to larger PAH molecules. In the spectrum of the soot without PAHs (after toluene extraction), a few small and distinct bands disappear and the overall spectrum becomes smoother (see gray solid curve). However, most of the features persist pointing to the fact that carbonaceous grains can show similar bands as PAHs. However, very large insoluble PAHs may also remain and contribute to the IR bands after extraction.

The spectral characteristics of LT condensates resemble the observed IR spectra of post AGB stars and protoplanetary nebulae (Kwok et al. 2001; Hony et al. 2003; Hrivnak et al. 2007). The comparison shown in Figure 5 clearly reveals that nearly all of the observed IR bands are also present in the LT condensate produced in the laboratory. Differences in band ratios, apparent for the  $=\text{C}-\text{H}$  out-of-plane vibrational bands in the range between 11 and 14  $\mu\text{m}$  for the condensate containing soot and PAHs, result from the overabundance of small PAHs, or larger PAHs containing outer rings with up to 4 to 5 H atoms compared to larger, compactly condensed species which should be more stable under astrophysical conditions. The pure soot particles (after extraction) which have consumed all the large PAHs during the growth process show a much better coincidence with the observed bands (see gray solid curve in Figure 5). The comparison reveals that the LT condensate is a promising dust analog for carbonaceous materials produced in carbon-rich AGB stars.

#### 4. CONCLUSIONS

The chemical pathways for the formation of carbon nanoparticles in HT and LT condensation processes are completely different, resulting in different structures and spectral properties of the condensed carbonaceous mat-

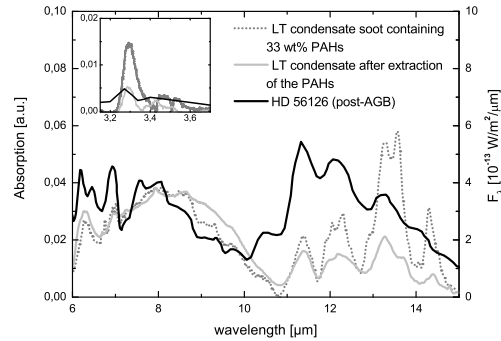


FIG. 5.— Comparison between the IR spectral properties of a LT condensate (LPcw3) and the observed spectrum of a post AGB star adapted from Hony et al. (2003).

ter.

The soot grains formed in HT condensation processes are characterized by very small particles with sizes up to 3-4 nm. Their structure can be described as fullerene-like soot grains containing elongated or symmetric cages, which can be interleaved. Most of the observed structural units are cage fragments which can be linked to another fragment either by aliphatic bridges or by van der Waals forces. The formation pathway of the soot particles is characterized by the formation of carbon chains that can form fullerene fragments of bowl shape with side chains. Long and branched carbon macromolecules are suggested to be the precursors for cyclic structures with long carbon chains attached which can condense and grow, for example, by a linkage of two linear chains attached to a nucleus (Irie et al. 2003).

A HT condensation process of carbon nanoparticles can be expected in supernovae (Clayton et al. 2001) or in the hot circumstellar environments of carbon-rich stars, such as Wolf-Rayet stars (Cherchneff et al. 2000).

In contrast, LT condensation realized by using cw laser-driven pyrolysis of hydrocarbons favors a formation process with PAHs as precursors and particle-forming elements, which condense on the surface of carbonaceous seeds via physi- and chemisorption. As a result, large carbonaceous grains are formed revealing well developed planar and slightly bent graphene layers in their interior. The samples produced in the present study are very valuable for a comparison with astrophysical data. Particularly noteworthy is the fact that LT laser pyrolysis experiments can produce a wealth of PAHs. The experimental conditions are comparable to those encountered in circumstellar environments around evolved stars (AGB stars) suggesting that, in these environments, the soot formation is governed by the synthesis of PAHs and their condensation on the surface of larger grains.

In circumstellar shells of AGB stars, the pressure is assumed to be lower than in the laboratory studies. However, our total pressure is not comparable to the total pressures in the atmospheres of dust-forming shells since we use a quenching gas to concentrate the condensation within a relatively small volume. The lower pressure in circumstellar condensation zones provokes the condensation to take place within longer distances and timescales

compared to laboratory experiments, however, it is not assumed that this results in a change of the condensate structure. HT condensation experiments performed in different pressures ranges (at  $\sim 3$  and  $\sim 300$  mbar) do not show a difference in the structure of the condensing species and, therefore, they support this assumption. Furthermore, we have to keep in mind that the graphite condensation is pressure-independent and much more sensitive to the C/O ratio in the dust-forming shells (Lodders & Fegley 1999). Furthermore, the condensation parameters and, in particular, the pressure as well as the degree of dust condensation can strongly vary in the dust-forming zone due to pulsations of the stellar interior (Nowotny et al. 2005b).

Low-temperature condensation is a very likely forma-

tion process of soot and PAHs in AGB stars. Condensation temperatures in our laboratory studies were found to be very similar to the temperature range for carbon dust condensation in carbon-rich AGB stars, predicted by Cherchneff & Cau (1999) to start at temperatures of 1700 K.

This work was supported by a cooperation between the Max-Planck-Institut für Astronomie and the FSU Jena as well as by the Deutsche Forschungsgemeinschaft (Hu 474/21-1). Furthermore, we would like to thank Dr. H.J. Räder, Max-Planck-Institut für Polymerchemie, Mainz, for the MALDI-TOF measurements.

## REFERENCES

- Allain, T., Sedlmayr, E., & Leach, S. 1997, *Astron. Astrophys.*, 323, 163
- Baum, T., Löffler, S., Löffler, P. H., Weilmünster, P., & Homann, K.-H. 1992, *Ber. Bunsenges. Phys. Chem.*, 96, 841
- Boulanger, F., Boissel, P., Cesarsky, D., & Ryter, C. 1998, *Astron. Astrophys.*, 339, 194
- Burtscher, H. 1992, *J. Aerosol Sci.*, 23, 549
- Buseck, P. R. 2002, *Earth and Planetary Science Letters*, 203, 781
- Buss, R. H., Snow, T. P., & Lamers, H. J. G. L. M. 1989, *Astrophys. J.*, 347, 977
- Cao, G. 2004, *Nanostructures and nanomaterials-Synthesis, properties and applications* (Imperial College Press), 51–63
- Cherchneff, I., Barker, J., & Tielens, A. 1992, *Astrophys. J.*, Part 1, 401, 269
- Cherchneff, I. & Cau, P. 1999, in *Asymptotic Giant Branch Stars: Proceedings of the IAU Symposium 191*, ed. T. Le Betre, A. Lèbre, & C. Waelkens (San Francisco:ASP), 251
- Cherchneff, I., Le Teuff, Y. H., Williams, P. M., & Tielens, A. G. G. M. 2000, *Astron. Astrophys.*, 357, 572
- Clayton, D. D., Deneault, E. A.-N., & Meyer, B. S. 2001, *Astrophys. J.*, 562, 480
- Dobbins, R. A., Fletcher, R. A., & Chang, H.-C. 1998, *Combustion and Flame*, 115, 285
- Doubenskaia, M., Bertrand, P., & Smurov, I. 2006, *Surface & Coatings Technology*, 201, 1955
- Draine, B. T. & Li, A. 2001, *Astrophys. J.*, 551, 807
- Drilling, J. S., Hecht, J. H., Clayton, G. C., et al. 1997, *Astrophys. J.*, 476, 865
- Drilling, J. S. & Schönberner, D. 1989, *Astrophys. J.*, 343, L45
- Foing, B. H. & Ehrenfreund, P. 1997, *Astron. Astrophys.*, 317, L59
- Frenklach, M. & Feigelson, E. 1989, *Astrophys. J.*, 341, 372
- Galazutdinov, G. A., Krelowski, J., Musaev, F. A., Ehrenfreund, P., & Foing, B. H. 2000, *Mon. Not. R. Astron. Soc.*, 317, 750
- Goel, A., Howard, J. B., & Vander Sande, J. B. 2004, *Carbon*, 42, 1907
- Granquist, C. G. & Buhrman, R. A. 1976, *J. Appl. Phys.*, 47, 2200
- Hecht, J., Holm, A., Donn, B., & Wu, C.-C. 1984, *Astrophys. J.*, 280, 228
- Heidenreich, S., Büttner, H., & Ebert, F. 2003, *Chemie Ingenieur Technik*, 75, 1787
- Henning, T. & Salama, F. 1998, *Science*, 282, 2204
- Homann, K.-H. 1998, *Angew. Chem.*, 110, 2572
- Hony, S., Tielens, A. G. G. M., Waters, L. B. F. M., & de Koter, A. 2003, *Astron. Astrophys.*, 402, 211
- Hrivnak, B. J., Geballe, T. R., & Kwok, S. 2007, *Astrophys. J.*, 662, 1059
- Iida, Y. & Yeung, E. 1994, *Appl. Spectr.*, 48, 945
- Irlé, S., Zheng, G., Elstner, M., & Morokuma, K. 2003, *Nano Letters*, 3, 1657
- Jäger, C., Kovacevic, E., & Strunskus, T. 2008a, *Carbon*, in preparation
- Jäger, C., Mutschke, H., Henning, T., & Huisken, F. 2008b, *Astrophys. J.*, 689, 249
- Jäger, C., Mutschke, H., Huisken, F., et al. 2007, *Carbon*, 45, 2981
- . 2006, *Astrophys. J. Suppl. Ser.*, 166, 557
- Jäger, C., Mutschke, H., Llamas-Jansa, I., Henning, T., & Huisken, F. 2008c, in *Organic Matter in Space; Proceedings of the IAU Symposium 251, held in Hong Kong 2008*, ed. S. Kwok & S. Sandford (SAO/NASA Astrophysics Data System), 425–432
- Kojima, H. & Naito, K. 1981, *Ind. Eng. Chem. Prod. Res. Dev.*, 20, 396
- Kroto, H. W. & McKay, K. 1988, *Nature*, 331, 328
- Kwok, S., Volk, K., & Bernath, P. 2001, *Astrophys. J.*, 554, L87
- Kwok, S., Volk, K., & Hrivnak, B. J. 1999, *Astron. Astrophys.*, 350, L35
- Lederer, M. T., Lebzelter, T., Aringer, B., et al. 2006, *Mem. S.A.It.*, 77, 1008
- Llamas-Jansa, I., Jäger, C., Mutschke, H., & Henning, T. 2007, *Carbon*, 45, 1542
- Llamas Jansa, I., Mutschke, H., Jäger, C., Schnaiter, M., & Henning, T. 2008, *Astrophys. J.*, in preparation
- Lodders, K. & Fegley, B., J. 1999, in *Asymptotic Giant Branch Stars; Proceedings of the IAU Symposium 191*, ed. T. Le Betre, A. Lèbre, & C. Waelkens (SAO/NASA Astrophysics Data System), 279
- Monier, R. & Parthasarathy, M. 1999, *Astron. Astrophys.*, 341, 117
- Mordkovich, V. Z. 2000, *Chem. Mater.*, 12, 2813
- Nowotny, W., Aringer, B., Höfner, S., Gautschi-Loidl, R., & Windsteig, W. 2005a, *Astron. Astrophys.*, 437, 273
- Nowotny, W., Lebzelter, T., Hron, J., & Höfner, S. 2005b, *Astron. Astrophys.*, 437, 285
- Nuccitelli, D., Richter, M. J., & McCall, B. J. 2006, in *Astrochemistry: Recent Successes and Current Challenges*, Proceedings of the IAU Symposium 231, ed. D. C. Lis, G. A. Blake, & E. Herbst (Cambridge University Press), 236
- Öktem, B., Tolocka, M. P., Zhao, B., Wang, H., & Johnston, M. V. 2005, *Combustion and Flame*, 142, 364
- Schnaiter, M., Gimmler, M., Llamas, I., et al. 2006, *Atmospheric Chem. Phys.*, 6, 2981, www.atmos
- Sellgren, K., Uchida, K. I., & Werner, M. W. 2007, *Astrophys. J.*, 659, 1338
- Smith, P. & Buseck, P. 1981, *Science*, 212, 322
- Vijh, U., Witt, A., & Gordon, K. 2005, *ApJ*, 619, 368
- von Helden, G., Hsu, M.-T., Gotts, N., & Bowers, M. T. 1993, *J. Phys. Chem.*, 97, 8182
- Weilmünster, P., Keller, A., & Homann, K.-H. 1999, *Combustion and Flame*, 116, 62
- Yeretzian, C., Hansen, K., Diederich, F., & Whetten, R. L. 1993, *Supplement to Z. Phys. D*, 26, 300
- Zheng, G., Irlé, S., & Morokuma, K. 2005, *J. Chem. Phys.*, 122, 014708